文章编号: 1001 - 9014(2017)04 - 0393 - 04

DOI:10.11972/j.issn.1001 - 9014.2017.04.003

Affects of flip-chip structure on the performance of THz detector with log periodic antenna

HAO Hai-Dong[1*], SHI Jun-Yu[1], CHENG Li-Feng[2], ZHAO Xiu-Chen[3], WANG Bing[1], LV Xin[1]

(1. Beijing Key Laboratory of Millimeter Wave and Terahertz Technology, School of Information and Electronics, Beijing Institute of Technology, Beijing 100081, China;
2. Institute of Microelectronics, Chinese Academy of Sciences (IMECAS), Beijing 100029, China;
3. School of Materials Science and Engineering, Beijing Institute of Technology, Beijing 100081, China)

Abstract: This paper presents a novel flip-chip (FC) structure design for 340 GHz Schottky diode detectors, which was designed and fabricated based on the gallium arsenide (GaAs) process. A ceramic thin-film supporting layer was used to provide a package for such detector. Conductive adhesive is typically used as attachment material between the antenna and output circuit. The behaviour of terahertz (THz) detectors with and without the novel FC structure was studied. For comparison, the FC structure model and wire bonding structure one (free of FC) were characterized using the same test system. A comparison analysis for the gains of the THz detector measured with and without the ceramic thin-film layer indicates that the novel FC structure offers a low-cost and practical solution for packaging the array of THz detectors.

Key words: THz, flip chip, log periodic antenna, THz package, thin-film ceramic, Schottky diode
PACS: 07.57.Kp

倒装焊结构对太赫兹对数周期天线的影响

郝海东[1*], 史君宇[1], 成立峰[2], 赵修臣[3], 王 兵[1], 吕 昕[1]

(1. 北京理工大学 信息与电子学院 毫米波与太赫兹技术北京市重点实验室, 北京 100081;
2. 中国科学院微电子研究所, 北京 100029;
3. 北京理工大学 材料科学与工程学院, 北京 100081)

摘要:设计了一种倒装焊结构,用于340 GHz的肖特基二极管探测器.探测单元是基于砷化镓(GaAs)工艺设计的.薄膜陶瓷支撑层旨在为太赫兹检测单元提供封装.通常,导电胶用作天线和输出电路之间的附接.分别对倒装焊结构和无倒装焊结构(类引线键合结构)模型对太赫兹接收天线性能的影响进行研究.为了比较的目的,使用相同的测试系统表征FC结构模型和无FC结构模型(引线键合结构).通过引线键合与倒装焊测试增益的结果比较,表明倒装焊结构可以作为大规模太赫兹检测阵列封装的低成本解决方案.

关 键 词:太赫兹;倒装焊;对数周期天线;太赫兹封装;薄膜陶瓷;肖特基二极管

中图分类号:TN454 **文献标识码**:A

Introduction

Terahertz (THz) band imaging provides vast potential for many attractive applications in the fields such as medicine, biology, security, and astronomy. The resolution of THz-scale imaging depends on the number of detector array elements in the system[1]. High quality, low-cost and practical packaging technology is thus required for these detectors. Field-effect transistor (FET)-based detectors are not faced with any packaging problem, but their current levels in the FET channels are relatively small compared with the noise current levels in typical biased source-drain channels, and also the detectors require lock-in amplifiers with narrow bandwidth in every channel[2]. Integrated planar THz antennas with Schottky

Received date: 2016-12-25, **revised date**: 2017-04-06 **收稿日期**:2016-12-25, **修回日期**:2017-04-06
Foundation items:Supported by China State 863 Projects (2015AA8123012, 2015AA8125024A)
Biography:HAO Hai-Dong (1986-), male, Beijing China, Ph. D. Research area is thin-film package processing for THz imaging device.
* **Corresponding author**:E-mail: issachao1226@gmail.com

diodes are important detector devices for THz focal plane imaging at room temperature[3]. Schottky-barrier diode (SBD) receivers have worse noise temperatures than both cooled hot-electron bolometer (HEB) receivers and superconductor-insulator-superconductor (SIS) mixers[4], but SBD operation without cooling offers opportunities to use SBD receivers in different mm-wave and sub-mm-wave applications. SBDs' sensitivity is well suited to mm-wave spectrometers with moderate resolution[5-7]. We therefore selected SBD detectors in this study. The THz radiation is focused using a silicon lens and is received by the antenna on the GaAs chip. The nonlinear device (i.e., SBD) that is integrated at the antenna's centre location is used to down-convert the THz signals to 10 MHz, so that they can be extracted via the output circuit.

To the best of our knowledge, the integration of a 340 GHz planar antenna with a stack structure containing a ceramic thin-film layer has not previously been reported. In this research, based on a previous successful demonstration of a 340 GHz FC structure simulation using a high frequency structure simulator (HFSS)[8], we proposed a silicon lens for coupling simulation with and without the FC structure model to carry out a comparison between the two structures. For a performance comparison, a single pixel of the FC model was fabricated and measured, and the radiation pattern results were then tested at 340 GHz. The FC structure model showed good agreement between its measured and simulated radiation patterns at 340 GHz.

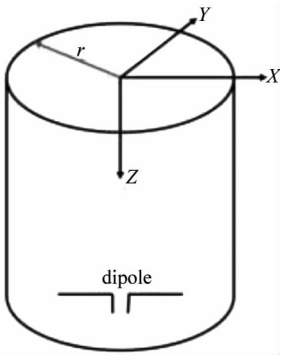

Fig. 1 Illustration of a dipole feed in a circular cylindrical cavity with the radius r

图1 偶极子馈电点在一个半径为 r 的圆柱空腔模型

1 Analysis of infinite circular cylinder cavity

It can help us easily determine the sensitivity parameter for the designed model to analyze the electromagnetic field distribution on the circular cylinder cavity. The solution assumes that the cavity is embedded in an infinite metallic circular cylinder with the radius $\rho = r$ (see Fig. 1). In this section, the finite element method is used to model the cavity, while the radiation condition is expressed using a boundary integral equation. The variational approach[9] and method of weighted residuals[10] can be used to accomplish the hybrid finite element-boundary integral equations. The derivation process begins with the three-dimensional vector wave equation that is determined in terms of the total electric field:

$$\nabla \times [\overline{\overline{\mu}}_{\gamma}^{-1} \cdot \nabla \times E] - k_0^2 \overline{\overline{\varepsilon}}_{\gamma} \cdot E = -jk_0 Z_0 J^{\text{int}} \quad (1)$$

where E is the total electric field, k_0 is the free-space wavenumber, Z_0 is the free-space impedance, $j = \sqrt{-1}$, and J^{int} is an interior current source. The material properties are expressed using the relative permittivity ($\overline{\overline{\varepsilon}}_{\gamma}$) and relative permeability ($\overline{\overline{\mu}}_{\gamma}$). A vector test function is used to test Eq. 1 and is integrated throughout the computational domain; the following solution is then obtained in the integrated form:

$$\int_V [\nabla \times W_i \cdot \overline{\overline{\mu}}_{\gamma}^{-1} \cdot \nabla \times E - k_0^2 W_i \cdot \overline{\overline{\varepsilon}}_{\gamma} \cdot E] \mathrm{d}V - jk_0 Z_0 \oint_s \hat{n} \times H^{\text{int}} \cdot W_i \mathrm{d}S = f^{\text{int}} \quad (2)$$

In Eq. 2, the interior excitation function is given by:

$$f^{\text{int}} = -jk_0 Z_0 \int_V J^{\text{int}} \cdot W_i \mathrm{d}V \quad (3)$$

for the sources such as dipole feeds. here the function was obtained from antenna-equivalent sources.

In this paper, the circular cylinder was assumed to be the computational volume. Therefore, the surface integral terms vanish at the walls of the cylinder when they lie on the surface where there is $\rho = r$. The expression is given in the following form:

$$\hat{\rho} \times H^{\text{int}} = \hat{\rho} \times H^{\text{ext}} = \hat{\rho} \times (H^{\text{inc}} + H^{\text{ref}}) + jk_0 Z_0 \int_{\text{Sap}} [\hat{\rho} \times \overline{\overline{G}}_{e2} \times \hat{\rho}'] \cdot E \mathrm{d}S' \quad (4)$$

where the natural boundary condition:

$$\hat{\rho} \times H^{\text{int}} = \hat{\rho} \times H^{\text{ext}} \quad (5)$$

is shown to be the connection between Eqs. 4 and 2. The exterior magnetic field has three component terms, which are the incident field (H^{int}), reflected field (H^{ref}) and aperture field in the cylinder respectively, as given by the surface integral shown in Eq. 4. In Eq. 4, the normal vector is given by $\hat{n} = \hat{\rho}$ because that the surface does not have a perfectly conducting face when $\rho = r$ exists. $\overline{\overline{G}}_{e2}$ is an electric dyadic Green's function of the second kind, which can be given as either a creeping wave serie[11] or an eigenfunction serie[12]. The relationships among the aforementioned equations showed that the circular cylinder radius r is a significant and sensitive design parameter in the cylindrical cavity radiation model; r enhances not only the Sommerfeld radiation condition but also the perfect electric conductor boundary condition on the surface of an infinite circular cylinder.

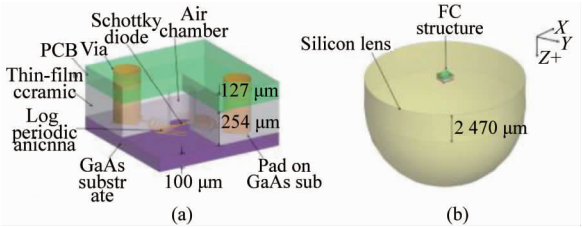

Fig. 2 Geometry of the proposed FC structure with the silicon lens (a) 3D cross-section of the FC structure, (b) 3D drawing of the FC structure and silicon lens configuration

图2 倒装焊模型和硅透镜的几何结构(a)倒装焊模型的3D截面,(b)倒装焊模型与硅透镜的3D图像

2　FC structure design and its configurations

The configuration of the proposed FC stack structure is shown in Fig. 2. The FC structure consists of three layers: a GaAs substrate as the top layer, a printed circuit board (PCB) as the bottom layer, and a ceramic thin-film central layer to support the entire structure. An air cavity was designed on the centre of the ceramic thin-film layer. Then an air chamber is located above the antenna area, and its diameter was optimized at 200 μm because of the design rule for the ceramic thin-film that requires the maximum through-via diameter to be less than the distance between two vias. Also, the smallest hole that can be processed in the ceramic thin-film layer is 200 μm in diameter. The antenna design parameters were given in our previous work[8]. The main dimensions of the FC structure and lens are shown in Table 1. Typical conductive adhesive is used to fill in the thin-film ceramic via structure with the negative pressure method with a masking film. Photographs of the mask layer and thin-film supporting layer are shown in Fig. 3.

Table 1　Main dimensions of the FC structure and Si lens
表 1　倒装焊封装结构和硅透镜的主要参数

Items	Dimension
GaAs substrate thickness	100 μm
Via diameter	200 μm
Air cavity diameter	200 μm
Distance between air cavity and via	200 μm
FC structure length and width	1,000 μm
Silicon lens diameter	13 mm

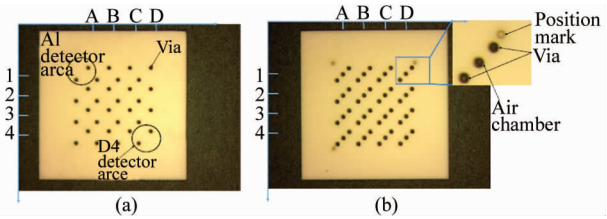

Fig. 3　Photographs of the mask layer and ceramic thin-film supporting layer (a) Mask layer, where the film mask material is the same as that of the ceramic thin-film supporting layer, (b) thin-film ceramic supporting layer
图 3　掩膜层照片和陶瓷薄膜支撑层照片(a)掩膜层所用材料与陶瓷薄膜支撑层一致,(b)陶瓷薄膜支撑层

3　Comparison of packages with and without the FC structure

Because the lens is too large in size for THz region simulation, the geometrical optical (GO) method has been selected for the lens simulation. First, the THz antenna structures with or without the FC structure were simulated using the commercial full-wave electromagnetic field (EM) simulation software FEKO, which is based on the coupling technique of finite element method (FEM)/multilevel fast multipole method (MLFMM), so as to scrutinize the radiation patterns of the two structures. Then, all far-field strength patterns of the different models were exported to act as new excitation sources for the lens simulation mode. The GaAs substrate, thin-film ceramic layer, and PCB were vertically stacked together, and their dielectric constants were assigned to be 12.9, 9.8 and 3.0 in the FEKO settings, respectively. The simulation results obtained at 340 GHz are shown in Fig. 4, where the FC structure with the 200 μm air cavity has similar gain to that of the model without the FC structure (wire bonding model), but the FC structure's radiation pattern is wider on the side face where Phi is equal to 0°. These results indicate that the ceramic thin-film dielectric has a horizontal guiding effect for THz waves in the *X-Z* plane; in addition, the *X-Z* plane is parallel with the diode's pole direction. However, the side face radiation pattern does not influence imaging applications.

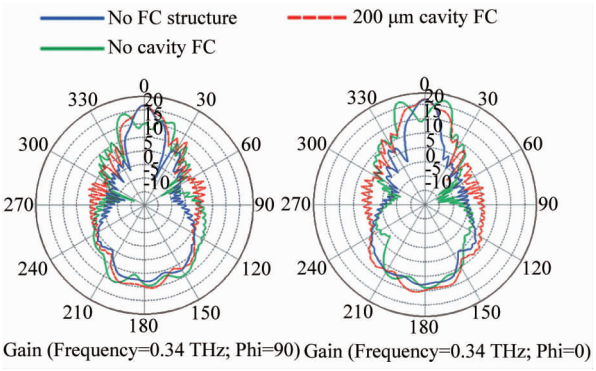

Fig. 4　Lens radiation patterns of the no-cavity FC model, proposed 200 μm cavity FC model and model without the FC (wire bonding model) at 340 GHz
图 4　所示分别为加透镜后无空腔的倒装焊结构,预设计 200 μm 直径空腔的倒装焊结构和金丝焊接结构方向图

4　Test results and discussion

Figure 5 presents a schematic of the THz array chip

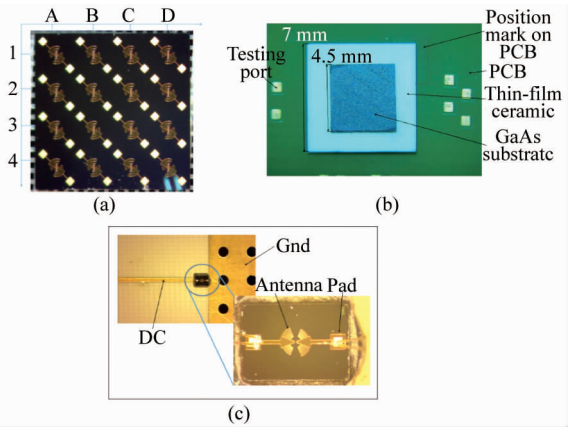

Fig. 5　Schematic of the THz array chip, and photographs of the FC and wire bonding structures (a) Schematic of THz array chip with the array size of 4 × 4, (b) photograph of the FC structure, (c) photograph of the wire bonding structure
图 5　THz 阵列芯片结构, FC 结构照片和金丝焊接结构照片(a)THz 阵列芯片:阵列规模 4 × 4,(b)倒装焊结构照片,(c)金丝焊接照片

and a photograph of the novel FC module. As the figure shows, the schematic was rotated to show the rear side of the THz array chip, which will be attached to the silicon lens to enable THz free space coupling. The test ports are placed on the PCB to demonstrate the electrical performance of the FC process. We selected the element B2 to make test comparisons and aligned the B2 cell with the optical axis of the silicon lens at 340 GHz.

The transmitting module is a '32 ×' planar Schottky diode frequency multiplier combined with a standard 340 GHz horn antenna. The receiving modules consist of THz Schottky diode detectors with the FC structure with the 200 μm air cavity or wire bonding structure. We adopted the THz modulation-demodulation testing method for the direct detector. A low-frequency spectrum analyser was used at the output port. The signal was generated and modulated at 10-MHz, carried by a 340 GHz carrier, and transferred in free space.

As a highly important parameter for imaging applications, the gain of the THz detector was obtained by recording the received power when the lens was focused on an emission source. The distance between the transmitting and receiving modules was modulated to allow the receiver to find the maximum far-field radiation location.

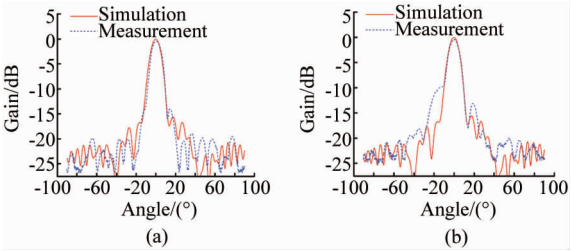

Fig. 6 Comparison of simulation and test results for the proposed FC model with the 200 μm air cavity at 340 GHz (a) Radiation patterns in the E-plane, (b) radiation patterns in the H-plane

图6 在340 GHz下200 μm直径空腔倒装焊模型的仿真和测试结果对比(a)E面方向图,(b)H面方向图

Figure 6 shows a comparison of the measured and simulated radiation patterns of the FC structure at 340 GHz. The 340 GHz horn antenna and frequency multiplier have typically narrow bandwidth. The received power expresses excessive attenuation at the output terminal when the frequency increases to more than 348 GHz. As shown in the figures above, satisfactory agreement is observed between the experimental and simulation results within the entire range of the antenna's main lobe. Additionally, the observed degree of main lobe correlation at 340 GHz is remarkable, given the complexity of the EM models, different processing structures, THz attenuation of the frequency multiplier and measurement setup. When a 200-μm-diameter cylinder cavity supporting layer is used, the B2 element pattern in the E-plane has a 3-dB beam width of $\theta_{3\text{-dB}} \sim 9.7°$, with side-lobe levels of less than -15 dB. The element pattern has $\theta_{3\text{-dB}} \sim 9.5°$ in the H-plane with the patterns as shown in Fig. 6 (b). The angular resolution, which is limited by the single pixel size and determined by the beam spacing, increases linearly with decreasing element spacing in both the E-plane and H-plane. However, increased angular resolution may cause the imaging contrast to deteriorate, particularly when the crossover power level becomes less than 3 dB[13]. Therefore, a fade in-out balance between the imaging contrast and imaging resolution must be achieved by selecting the appropriate element size in the planar THz focal plane array (FPA).

5 Conclusion

A novel FC structure operating in the THz band that is based on processing of a ceramic thin-film stack layer was designed, fabricated using the typical FC equipment, and subsequently tested. The measured radiation pattern showed good agreement with the corresponding simulated results at 340 GHz. These results indicate that the proposed FC structure is an efficient and inexpensive package structure for THz imager assembly. It should also be noted that the ceramic thin-film structure can provide excellent protection for the diode air bridge without the needs to create an under bump metal (UBM) layer or perform underfill processing.

Acknowledgements

This work was supported by the Chinese Academy of Sciences and the State Key Laboratory of Millimetre Waves.

References

[1] Komiyama S, Astafiev O, Antonov V, *et al*. A single-photon detector in the far-infrared range [J]. *Nature*, 2000, **403**(6768): 405 - 407.
[2] Ojefors E, Pfeiffer U R, Lisauskas A, *et al*. A 0.65 Thz focal-plane array in a quarter-micron CMOS process technology [J]. *Solid-State Circuits*, 2009, **44**(7):1968 - 1976.
[3] Maiwald F, Lewen F, Vowinkel B, *et al*. Planar Schottky diode frequency multiplier for molecular spectroscopy up to 1.3 Thz [J]. *IEEE Microwave and Guided Wave Letters*, 1999, **9**(5): 198 - 200.
[4] Hübers H W. Terahertz heterodyne receivers [J]. *IEEE J. Sel. Top. Quant*, 2008, **14**:378 - 391.
[5] Setzer C S, Mattauch R J. High-performance millimetrewave GaAs Schottky-barrier flip-chip diode [J]. *Electronics Letters*, 1981, **17**(16): 555 - 557.
[6] Crowe T W, Mattauch R J, Roser H P, *et al*. GaAs Schottky diodes for Thz mixing applications [J]. *Proceedings of the IEEE*, 1992, **80**(11):1827 - 1841.
[7] Erickson N R. Low-noise submillimeter receivers using single-diode harmonic mixers [J]. *Proceedings of the IEEE*, 1992, **80**(11):1721 - 1728.
[8] Hao H D, Tang Z, Lv X. Simulation of a novel flip-chip antenna in Thz region [C]. *Advanced Materials and Processes for RF and THz Applications* (*IMWS-AMP*), 2015.
[9] JIN J M. *The finite element method in electromagnetics* [M]. Wiley/Interscience, New York, 1993.
[10] Volakis J L, Chatterjee A, Kempel L C. *Finite element method for engineering: Antennas, microwave circuits, and scattering applications* [M]. IEEE Press, New York, 1998.
[11] Prabhak P H, Wang N N. *An analysis of the mutual coupling between antennas on a smooth convex surface* [M]. Ohio State University ElectroScience Laboratory Technical Report, 1978, **784583**:7.
[12] Tai C T. *Dyadic green's functions in electromagnetic theory* [M]. IEEE Press, New York, 1994.
[13] Filipovic D F, Gauthier G P, Raman S, *et al*. Off-axis properties of silicon and quartz dielectric lens antennas [J]. *IEEE Trans. Antennas Propaga*, 1997, **45**(5): 760 - 766.